Scientific
Research
Publishing

Effects of the Produced Water from a Sour Oilfield in South Kuwait on the Production Tubing

Feras Al Salem[1], Vijo Poulose[2], Kazuyuki Kawamura[3], Arata Nakamura[3], Hakim Saibi[4], Thies Thiemann[2]*

[1]Department of Biology, College of Science, United Arab Emirates University, Al Ain, United Arab Emirates
[2]Department of Chemistry, College of Science, United Arab Emirates University, Al Ain, United Arab Emirates
[3]Technology and Research Center, Japan Organization for Metals and Energy Security (JOGMEC), Chiba, Japan
[4]Department of Geosciences, College of Science, United Arab Emirates University, Al Ain, United Arab Emirates
Email: thies@uaeu.ac.ae, *thiesthiemann@yahoo.de

Abstract

Kuwaiti oil production faces a growing challenge in the increasing quantities of produced water generated in the production of oil. The high water cut of the produced fluid from the wells and the high salinity of the produced water lead to significant degradation of subsurface equipment, specifically the production tubing. Debris generated through the degradation of the inner part of the tubing becomes a constituent of the scaling that deposits in the tubing and blocks the flow of the production fluid, inducing higher maintenance costs. This paper looks at the characteristics of the scaling in regard to the produced water and outlines the economic impact of the produced water induced degradation of the tubing structure.

Keywords

1. Introduction

Produced Water (PW) is the water associated with oil during the extraction process [1]. In oil and gas formations, the subsurface rocks are mostly filled with fluids such as water, oil and/or gas, or some combination of these three main components. Thus, oil and gas reservoirs often contain both formation water as well as hydrocarbons [2]. PW includes a number of water-soluble and insoluble

organic and inorganic compounds [3], and is considered one of the largest streams of generated wastewater. The global annual production of produced water is estimated to have reached 250 million barrels per day in 2020 [4]. Amongst the compounds found in PW are inorganic salts and a wide range of oil related hydrocarbon compounds. The type and concentration of metal and metalloid salts in PW vary widely and depend on the age and geology of the oil and gas field [5]. It is important to treat the produced water associated with the crude oil operations, where this water upon reinjection into the production zone may affect the quality of the oil, its properties, and therefore its price [6]. If not re-injected but disposed of, environmental considerations are of primary concern. In this regard, purifying the produced water to such a degree that it can be re-injected into the production zone or that it can be utilized for another purpose rather than stored, contributes to sustainable resource management by reducing the generation and accumulation of waste [7]. In our study of possibilities of purifying produced water from a Kuwaiti oil production site, we initially studied the impact of the produced water on the operation, focusing on potential damages to the subsurface equipment, specifically the production tubing, which carries the production fluid from the subsurface to above-ground. Corrosion of the tubing that carries the production fluid is a major worry [8]-[14] when, evaluating the structural integrity of the oil production facility. It has been noted that as many as 33% [15] to 51% [16] of oil/gas pipeline failures are caused by corrosion of the pipes [13] [14]. It has been reported that in the case of produced water from sour oil/gas fields tubing, failures are frequent and the workover rate significant [8].

The focus of this study is an oilfield located in South Kuwait. It is a mature field with a water cut of 1:4. Production from 40 - 60 different wells is combined to supply a central processing substation (Figure 1). The total field is comprised of over 1000 wells.

The tubing in use in the subsurface is made of steel (for details, please consult Table 1). A typical length of tubing used from the active production zone to the central process unit is in the range of 300 m - 675 m, with a total tubing for the complete operation connected to one substation of about 40.000 m (Figure 2).
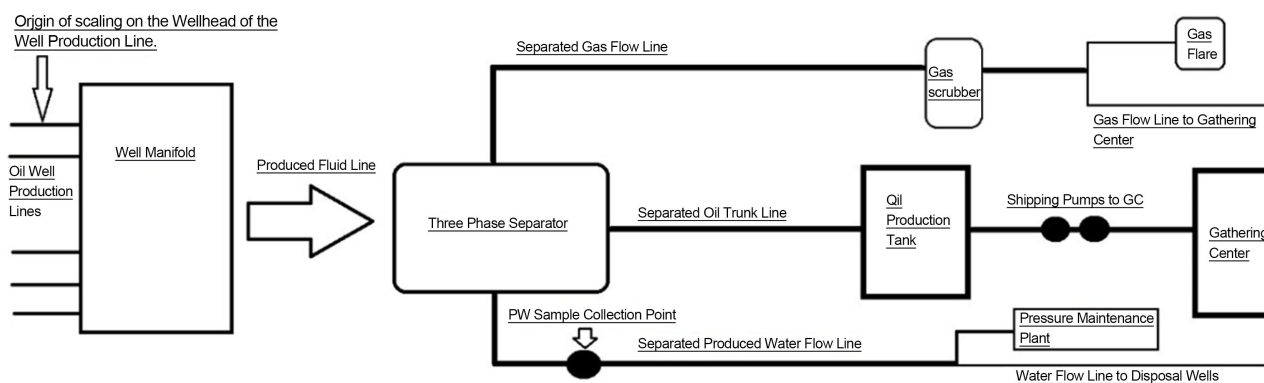
Figure 1. Flow chart of the liquid and gas streams in a typical Kuwaiti production site, where oil, gas and produced water from different wells are centrally connected.
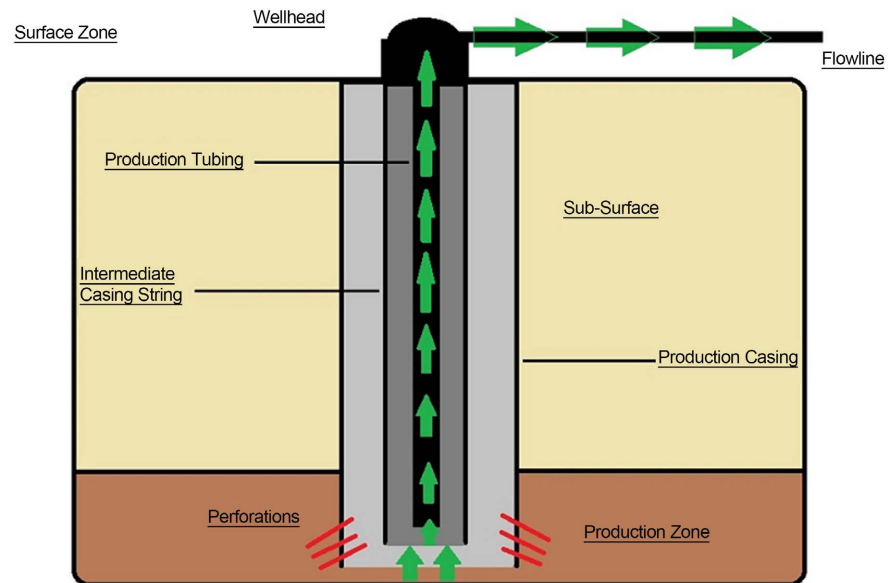
Figure 2. Kilometers of metal tubing are used to transport the oil/gas (in addition to produced water) to the surface.

Table 1. Chemical composition of the tubing material, mass fraction (%) – the remainder is Fe. [a]The carbon content may increase to 0.5% if the tubing is oil-quenched.

C	Mn	Ni	Cu	P	S	Si
0.43[a]	1.90	0.25	0.35	0.030	0.030	0.45

The scale formation in pipe tubing in oil and gas fields is influenced by a number of factors such as the nature of the produced water, the temperature [17], pressure [18], pH [19], and flow velocity [20] [21]. Due to its high ion content, especially the high chloride [22], but also calcium content [23], produced water is corrosive to metals. In addition, produced water from sour oilfields often has a relatively low pH [24] which again supports metal corrosion [25]. Because of this reason, 50% of tubing has to be exchanged every 6 months at a cost of $12.9 per tubing meter (**Figure 3**). The corrosion adds to non-soluble particles in the produced water and leads to additional scaling within the tubing. The scale and residual material block the production tubing's inner space, which prevents the oil from flowing from the production zone to the surface (**Figure 4**). This causes a drop in the well's productivity and requires a workover job to be performed on the well to restore its production capacity.

The current contribution looks at the impact of the produced water on the production tubing, investigates the composition of the deposits on the inner surface of the tubing, and the composition of the scaling. The work focuses exclusively on the subsurface tubing and not on the tubing above ground. The tubing above ground has different characteristics than that in the subsurface, both in steel composition and dimensions, including the thickness (9.5 mm above-ground vs. 5.7 mm in the subsurface), that makes the tubing above ground less prone to fail. Some of the questions that were looked at in this study

Figure 3. Visuals of corroded subsurface production tubing at end of life.

(a)	(b)	(c)
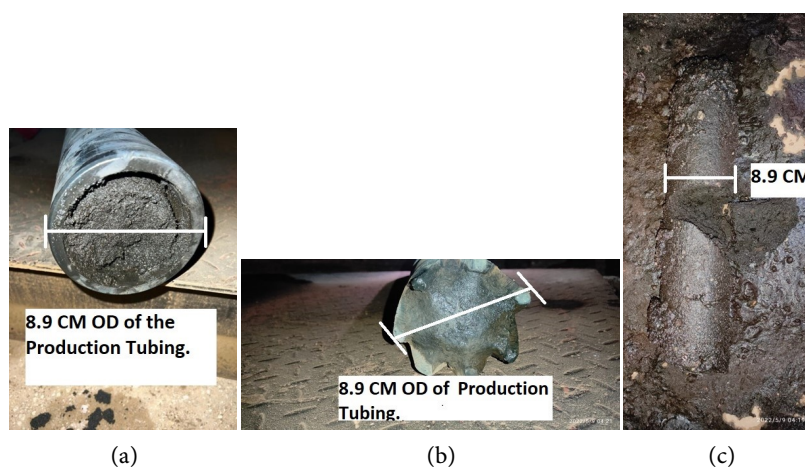
Figure 4. (a) Scale forming in different intersections of the production tubing prior flushing. (b) Scale and residual material blocking the production tubing of a well in Kuwait. (c) Scale and residual material found inside of production tubing of an oil well in Kuwait.

were what contribution the metal debris from the pipes would make to the overall scaling, what iron compounds would be included in the scaling, whether sulfidic iron compounds would be included in the scaling and whether one could observe evidence of chloride induced corrosion.

2. Materials and Methods

Produced water samples, tubing, including connection pieces and scaling samples [*in this contribution, solids that have deposited on the surface on the tubing as well as debris stemming from the tubing that has lodged itself in the tubing is seen as scali*ng] were sourced from a production site in a sour oilfield in South Kuwait. The produced water analysis was carried out at the CORE labs, Abu Dhabi, UAE. The surface textures of the scaling samples and the tubing were investigated with a stereo microscope (Model SZ2-ILST) and a scanning electron microscope (SEM, Thermo Quattro S). As the raw scalings were coated with hydrocarbons and other carbonaceous material, raw scalings were submitted to

"ashing" at 600˚C in a Carbolite oven, in order to evaluate the inorganic composition, including the metal content and metal salts. Also, raw scalings were extracted with toluene at rt. Regarding visual textural analysis of scalings and tubing, photos or micrographs were taken with a stereoscope (Model SZ2-ILST) and a scanning electron microscope. Regarding spectroscopic analysis, Fourier-Transform infrared (FT-IR) spectroscopy of the samples was carried out with a Perkin Elmer Spectrum 2 FT-IR spectrometer. WD-XRF spectra on the samples were performed with Rigaku Primus IV. XPS spectra on the samples were carried out with a Nexsa G2 (Thermo Scientific, UK). In addition, SEM was performed in combination with energy dispersive X-ray spectroscopy (EDS).

Collection of produced water, scaling, and tubing. - Two samples of produced water (20 L each) were collected from a production facility in Kuwait in November 2021 and in January 2023. Three samples of scaling (200 g each, named here scalings 1 - 3) were collected from a production tubing assembly that carried oil and produced water as well as small amounts of gas at the same production facility in January and in February 2023 (Figure 2). For this, production piping (diameter: 3.5 inches) was dissembled (Figure 3, Figure 4), and the scaling was flushed with diesel. Before collection, the diesel was evaporated from the scaling. In addition, the authors received a completely de-oiled scaling sample from the same production site (here, named scaling 4). A short section of a used tubing piece at end-of-life was obtained from the production site. Pieces of the tubing were mechanically cut to mount them for the necessary analytical analyses.

Determination of the composition of the scaling and the tubing. – The scaling which included some remaining moisture contained both hydrocarbons and metal salts. To determine the moisture and volatile content, the scaling samples were heated to 120˚C for 24 h in a Carbolite oven (ELF 11-6) with a weighed sample of each product placed in a crucible (79C-00, Waldenwanger, Berlin). The moisture/volatile contents are expressed in w% within the text. A triplicate of experiments was carried out and the values are given as average values ± standard deviation. To determine the metal content, the scaling was heated at 600˚C for 3 h with a weighed sample of each product placed in a crucible (79C-00, Waldenwanger, Berlin). The ash contents are expressed in w% within the text. A triplicate of experiments was carried out and the values are given as average values ± standard deviation. As metal salts can potentially react under the ashing conditions, especially iron sulfide to iron oxide and low valency iron species to iron (III) oxide, an extraction of the raw scalings with toluene was performed. For this, scalings (ca. 10 g) were weighed into a round-bottom flask, toluene (70 mL) was added and the resulting suspension was stirred at rt for 4 h. The toluene solution was decanted, and the process was twice repeated with 70 mL toluene, each. Finally, the extracted scalings were filtered off and dried in an EcoCell drying cabinet at 37˚C for 12 h. A triplicate of experiments was carried out and the values are given as average values ± standard deviation. The cooled ash and toluene extracted samples were subjected to wavelength dispersive X-ray fluorescence spectroscopy (WD-XRF), powder X-ray diffraction (P-XRD), scan-

ning electron microscopy coupled with energy dispersive X-ray spectroscopy (SEM-EDS), X-ray photoelectron spectroscopy (XPS) as well as to FT-IR spectroscopy (FT-IR).

Wave-length dispersive X-ray fluorescence (WD-XRF) -The elemental composition of each sample was analyzed using a wavelength dispersive X-ray fluorescence (WD-XRF) instrument (Rigaku ZSX Primus IV, Japan) equipped with a Rh X-ray tube and controlled by ZSX guidance software. The sample was placed on a specified sample holder cup and analyzed directly.

Powder X-Ray diffraction analysis (P-XRD)—The powder X-ray diffraction analysis was recorded on a Rigaku Miniflex XRD, Japan, where the diffraction patterns of the samples were recorded with a Bragg's angle 2θ from 5° to 90° using Cu Kα radiation (λ = 1.54 Å) at voltage 45 kV and 40 mA current. All the analyses were performed at ambient temperature.

Scanning electron microscopy coupled with energy dispersive X-ray spectroscopy (SEM-EDS)—SEM images were captured with a Thermo Quattro S instrument at high vacuum mode (6×10^{-4} Pa), with an accelerating voltage of 30kV and using an Everhart-Thornley SE detector (ETD). The EDS analysis was performed with an energy dispersive X-ray detector attached to the SEM.

X-ray photoelectron spectroscopy (XPS)—A photoelectron spectrometer Nexsa G2 (Thermo Scientific, UK) was employed in the conducted studies to examine the elemental composition and chemical state of the samples. The instrument utilized monochromatized Al-Kα radiation (1486.6 eV) with a spot size of 400 μm and employed a flood gun for static charge compensation. Survey spectra were acquired with a pass energy of 200 eV, while high-resolution scans were conducted at 50 eV, all under an ultra-high vacuum environment of approximately 10^{-9} mbar.

Fourier Transform infrared spectroscopy (FT-IR)—The FT-IR spectra were obtained using a Perkin Elmer Spectrum Two Spectrometer and the data were processed using Spectrum IR software. For sample preparation, IR grade KBr (Aldrich) was mixed with the sample and the transmittance of the ensuing KBr sample pellet was recorded in the range 4000 - 500 cm^{-1} and processed after 32 scans.

3. Results

3.1. Water Quality Analysis

Table 2 lists the ion concentrations of a typical produced water sample gathered for this research in the sampling process. One can note a high overall concentration of total dissolved solids (TDS) of 132,780 mg/L. The ion concentrations of sodium (Na$^+$) with 35,600 mg/L and chloride (Cl$^-$) with 75,660 mg/L are high, but still well below known upper limits of concentrations in produced water for Na$^+$ (250,000 mg/L) and Cl$^-$ (150,000 mg/L) [4]. Also, the concentrations of potassium (K$^+$) with 1520 mg/L, magnesium (Mg^{2+}) with 1730 mg/L, and calcium (Ca^{2+}) with 7670 mg/L are notably high. Moreover, the concentrations of total iron (1.36 mg/L) and also of "dissolved" iron (Fe, 0.44 mg/L) are appreciably

Table 2. Properties and ion content of a typical produced water under investigation from a Kuwaiti sour oilfield.

		Raw Kuwaiti produced water sample
TSS (0.45 μm)		11
Total Dissolved Solids		132,780
Dissolved Oxygen (ppm)		3
pH at 25°C		6.88
Cations	Sodium	35,600
	Potassium	1520
	Calcium	7670
	Magnesium	1730
	Barium	2.3
	Strontium	255
	Total Iron	1.36
	Dissolved Iron	0.44
Anions	Chloride	75,660
	Sulphate	18
	Bicarbonate	140
Additional Components	Silicon	12.3

elevated, most likely due to the corrosion of the tubing infrastructure. There is little evidence of sulfur containing species, with sulphate (SO_4^{2-}) at only 18 ppm. The pH of the produced water of 6.88 is at the higher end of reported pH values for produced water from this type of oilfield in general [26]. It is known, however, that during laboratory storage the pH of the produced water may rise and thus the pH of the water in the reservoir can probably be appreciably lower. Previously, pH values of produced water from other Kuwaiti oil fields have been reported in the range of pH 6.4 - 6.5 [4]. pH 6.5 is also the pH value of the investigated produced water after filtration through a ceramic membrane. The pH of produced water can be influenced by chemicals used in the production [27] and may also change as the field ages [28].

3.2. Spectroscopic Analysis of the Scaling Samples

The scaling samples [*in this contribution, solids that have deposited on the surface on the tubing as well as debris stem-ming from the tubing that has lodged itself in the tubing is seen as scaling*] collected from different blocked locations in the subsurface tubing structure, after dissembling the tubing, differ from each other in their share of volatiles, hydrocarbon content and water content (Table 3). In themselves, the scalings were found to be relatively heterogeneous. Scaling 4 was obtained as a completely de-oiled, dry sample, and thus showed more homogeneity. In the chemical composition, as analyzed by wave-length dispersive X-ray fluorescence spectroscopy (WD-XRF), ashed scalings differed signifi-

cantly from each other (Table 4), although all of the scalings majorly consisted of material debris from the tubing itself, as evidenced by the iron content of the samples (63.7 - 95.3 w%). In all scaling samples, there was a heightened sulfur (2.9-19.6 w%) and calcium content (0.8 - 9.3 w%).

WD-XRF analysis of a pristine tubing surface showed, apart from Fe (96.0 w%), the presence of Mn (1.6 w%), Si (1.2 w%) and Al (1.4 w%) (Table 5). Mn and Si are constituents of the metal piping (Table 1). Also, the source of Al is most likely the metal tubing itself as Al content (1.4 w%) has been found by us in the tubing material, although it is not listed in the tubing's API specification (Table 1). WD-XRF analysis of the inner side of the used tubing shows a much more complex composition. The analysis was performed in a semi-quantitative mode and each element is compared in regard to its identity with characteristic X-ray fluorescence spectra.

Table 3. Macroscopic constitutional characteristics of scalings 1 - 3, extracted from the production tubing. Scaling sample 4 was a completely de-watered, de-oiled sample.

Sample	Scaling 1	Scaling 2	Scaling 3
Volatiles	23.74 ± 0.12 w%	1.02 ± 0.07 w%	8.43 ± 0.50 w%
Ash content	61.32 ± 2.74 w%	84.29 ± 0.32 w%	68.63 ± 0.36 w%
Toluene extractable solids	25.97 ± 1.84 w%	10.21 ± 1.84 w%	34.57 ± 1.92 w%
Water and Toluene non-extractable organic Content	12.71 w%	5.5 w%	ND

Table 4. The inorganic content of a typical scaling collected from a tubing in the subsurface as determined by WD-XRF spectroscopy of the sample ashes at 600°C (elemental composition was measured as the respective oxides).

Sample	Scaling sample 1	Scaling sample 2 (ashed)	Scaling sample 3 (ashed)	Scaling sample 4 (ashed)
Components	Result (w%)	Result (w%)	Result (w%)	Result (w%)
Mg	ND	0.159	1.63	ND
Al	ND	0.391	2.12	2.4
Si	ND	3.39	7.29	8.5
P	ND	0.014	ND	ND
S	2.78	19.6	11.6	4.8
Cl	ND	0.091	0.23	1.4
K	ND	0.411	0.67	ND
Ca	1.97	0.754	9.30	3.5
Mn	ND	0.700	0.55	ND
Fe	95.3	74.4	63.7	79.5
Cu	ND	0.121	1.13	ND
Zn	ND	ND	1.41	ND
Pb	ND	ND	0.14	ND

Table 5. The inorganic content of the surface of the inner wall of the production tubing and of the pristine surface of a newly cut production tubing as determined by WD-XRF spectroscopy of the mounted samples.

Sample	Mg (w%)	Al (w%)	Si (w%)	P (w%)	S (w%)	Cl (w%)	Ca (w%)	Fe (w%)	Zn (w%)	Mn (w%)
Inner tubing	2.9	2.4	8.1	1.7	1.4	1.9	5.8	64.0	11.8	ND
Cut cross section	ND	1.4	1.2	ND	ND	ND	ND	96.0	ND	1.6

As with the WD-XRD analysis (see above), an EDS (energy dispersive X-ray spectroscopy) analysis (Figure 5, Table 6) of the pristine surface of the tubing (Figure 5(b)) revealed an elemental composition of the tubing similar to that given in the API specification of the tubing, in addition to a small amount of Mg. The EDS analysis of the inner tubing at end-of-life that was exposed to the produced fluid, showed an expected number of elements that can also be found in the produced water (Table 2) including S, P, Cl, Na, and K. With 5.8%, there is a heightened concentration of Ca. The EDS analysis of the scaling shows similar elements, with a noted absence of Zn. The presence of Zn on the surface of the inner tubing is discussed below.

X-ray photoelectron spectra (XPS) of scalings were performed in order to assess changes in the composition of the scaling during the ashing process (Figure 6), and it could be ascertained that the mineral composition of the ashed samples resembles the mineral composition of the original scalings. XPS of the cold extracted scaling shows $Fe(0)$, $Fe(II)$ and $Fe(III)$ species, while the ashed sample was mostly composed of $Fe(III)$ species and $Fe(II)$ species, with $Fe(0)$ no longer in evidence. Apart from that, changes of the metal salts are moderate. Thus, greigite and goethite have been found in both the ashed and the cold extracted scalings.

The main absorption bands in the FT-IR spectrum (Figure 7) of a scaling sample, can be seen to stem from Fe_2O_3 (551 cm^{-1}) and from silica (1128 cm^{-1}). XRD of an ashed sample of scaling 2 showed diffraction peaks of magnetite (Fe_2O_3; $2\Theta = 36.63°$, $44.13°$, $57.20°$, $63.06°$), hematite (Fe_2O_3; $2\Theta = 33.91°$, $36.44°$, $54.59°$), greigite (Fe_3S_4, $2\Theta = 30.06°$, $36.63°$, $52.32°$), siderite ($FeCO_3$, $2\Theta = 33.00°$) and goethite (α-FeO(OH), $2\Theta = 7.45°$, $36.63°$).

3.3. Textural Analysis of the Scaling Samples and Energy Dispersive X-Ray Spectroscopic (EDS) Measurements in Combination with Scanning Electron Microscopy (SEM)

Samples of the pristine newly cut tubing sample (Figure 8, row 1), inner exposed surface of tubing (Figure 8, row 2) and scale sample 4 (Figure 8, row 3) were collected and their morphologies were studied by SEM. Figure 8 shows digital camera photos (Samsung Galaxy A51), stereoscope images and SEM micrographs of the three samples, respectively.

The SEM micrograph of the newly cut surface of the tube shows a uniform texture with ridges and indentations stemming from the cutting process (Figure 9(a)). The EDS results show a very similar composition at every point of the surface

(a)

(b)

(c)
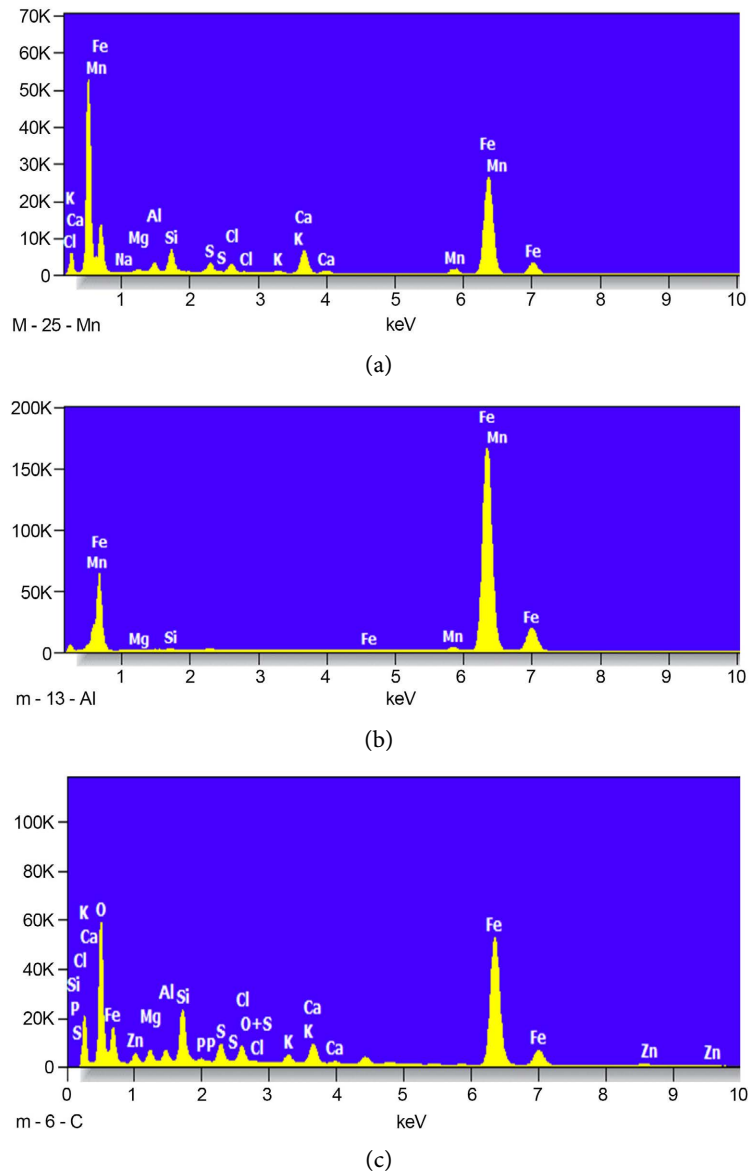
Figure 5. EDS (energy dispersive X-ray spectroscopy) spectra of a scaling sample (a); newly cut surface of the tubing (b); and the inner, exposed surface of the tubing (c).

Table 6. The elemental composition of the surface of (first row) scaling 4, (second row) the pristine, newly cut piping piece; and (third row) the exposed inner tubing as determined by electron dispersive X-ray spectroscopy (EDS).

| SAMPLE	O (w%)	Na (w%)	Mg (w%)	Al (w%)	Si (w%)	P (w%)	S (w%)	Cl (w%)	K (w%)	Ca (w%)	Mn (w%)	Fe (w%)	Zn (w%)
Scaling 4	27.9	1.1	0.5	0.2	0.7	ND	1.5	2.2	0.3	5.2	ND	60.3	ND
Newly cut surface	ND	ND	ND	ND	0.3	ND	ND	ND	ND	ND	1.4	98.3	ND
Exposed inner tubing	36.2	ND	2.6	1.6	6.4	0.3	2.0	2.0	1.0	2.6	ND	43.9	1.4

(a)

(b)
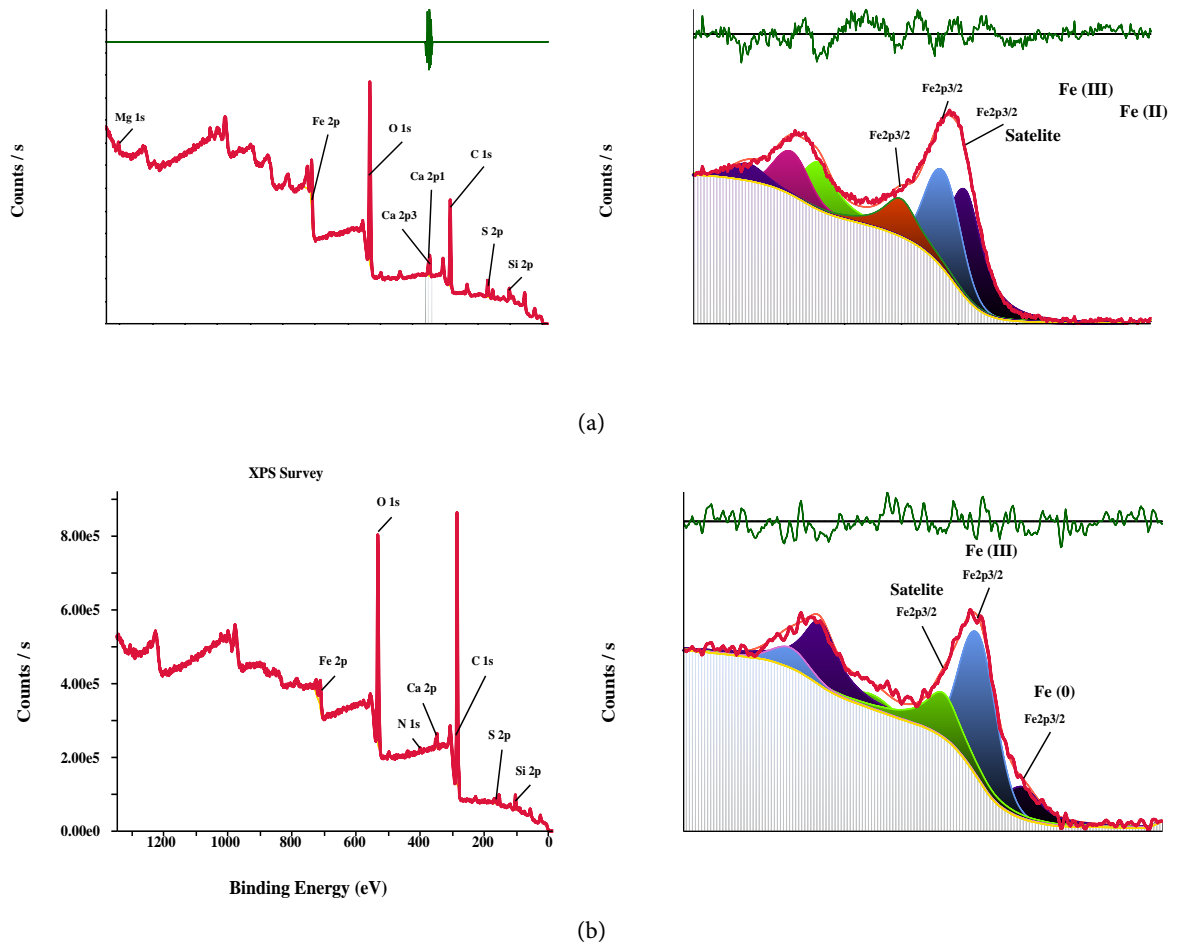
Figure 6. X-ray photoelectron spectra (XPS) of ashed and cold extracted scalings. (a) X-ray photoelectron spectrum of the ashed scaling sample showing Fe(III) with smaller amounts of Fe(II) species in the sample; (b) X-ray photoelectron spectrum of a toluene extracted scaling sample showing Fe(0), Fe(II), and Fe(III) species in the sample.
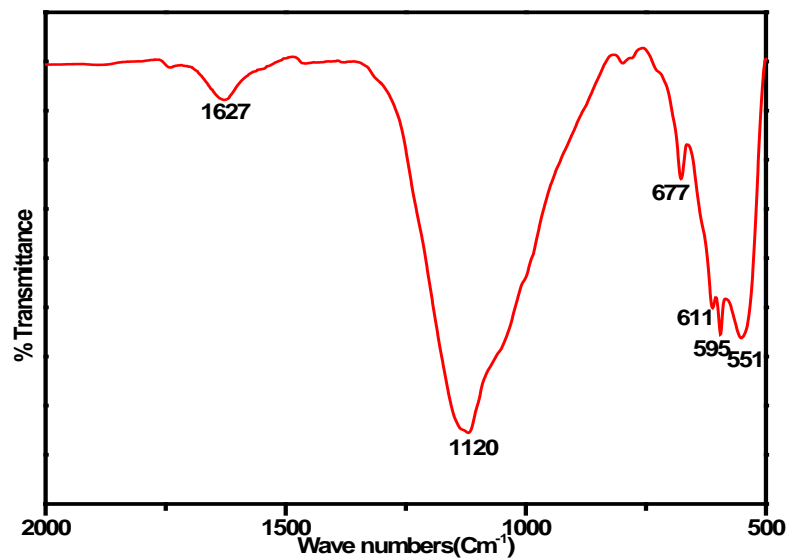
Figure 7. Infrared of a scaling sample.
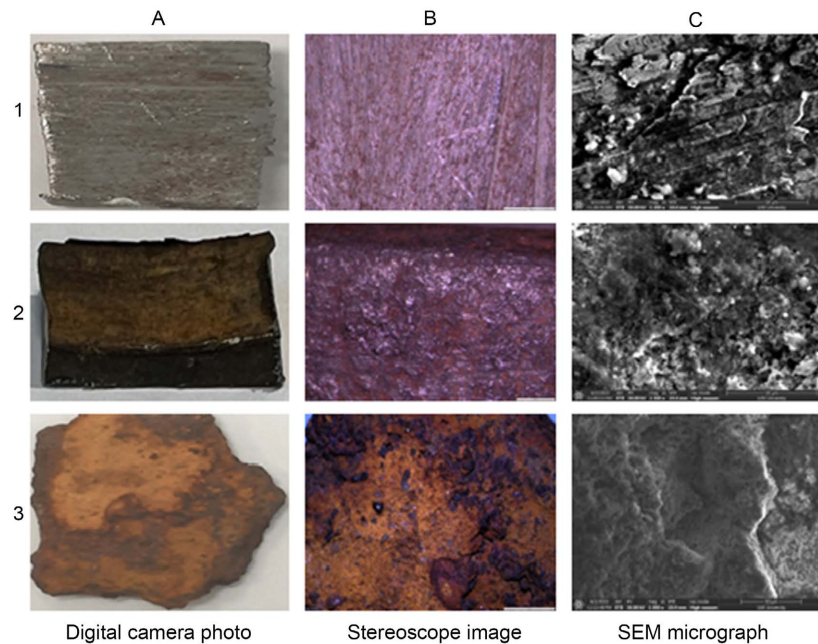
Figure 8. Digital camera photos taken with Samsung Galaxy A51 (column A), stereoscope images taken with stereoscope (Model SZ2-ILST, column B) and SEM micrographs (column C). Depictions in row 1 represent the newly cut surface of the tube, in row 2 the inner exposed surface of the tube and row 3 the scaling sample 4.
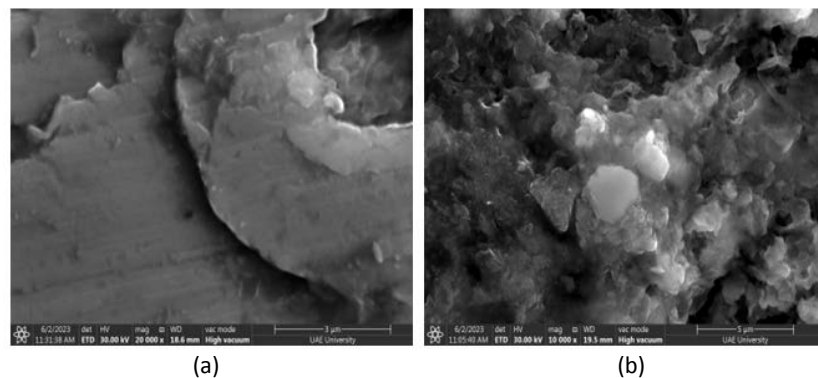

Figure 9. (a) SEM analysis of a newly cut, pristine surface of the tubing at magnification X 20,000, 3 μm and (b) of the inner exposed surface of the tube at magnification X 10,000, 5 μm.

that was investigated. The composition is within the range given by the specifications of the tubing as shown in Table 1, except for a slightly elevated value of silicon, which may be due to the desert environment the tubing is exposed to. The major component is iron, together with 1.6 mass% of manganese (Mn) and a small percentage of silicon. The SEM image (Figure 9(b)) of the inner exposed surface of the used tubing shows a much rougher surface with crystalline structures which by EDS (Figure 5(c)) were revealed to have higher silicon and higher chloride content. Sulfur, mostly as sulfidic sulfur and as sulfate, is in evidence (Figure 5(c)). As metal cations, magnesium (Mg), calcium (Ca), potassium (K), and sodium are found (Na). All four are dominant cations found in the produced water samples as

well (**Figure 5(c)**). In addition, aluminum (Al) and zinc (Zn) were found. Zinc may stem from the crude itself [4]. Both elements were also found in the WD-XRF measurements. It must be stressed that WD-XRF is a semi-quantitative analytical technique, where 1 mm² of the surface is characterized. In the case of our EDS analysis, single point measurements were carried out, and this can be more of a qualitative elemental analysis. Each element line in the EDS spectrum is compared with its corresponding keV values of Kα, Kβ and Lα.

SEM analysis shows a relatively smooth texture of the freshly cut tubing surface (**Figure 9(a)**). The inner exposed surface of tubing looks significantly rougher. Crystallites lodged into the surface or deposited onto the surface are in evidence (**Figure 9(b)**). The scaling samples were also examined by SEM (**Figure 10** and **Figure 11**). Individual scales, which oftentime represented lodged debris from the tubing, exhibit a crystallized ridge of salt with a heightened chloride content (**Figure 10**). The scales show ordered, regular rows of pits, some of which have progressed to the state of perforations. Different sized pits/perforations are visible in the SEM images with the larger having diameters of 30 - 68 μm (**Figure 10(b)**, **Figure 11(b)**) and the smaller having a diameters of 1.0 -3.3 μm (**Figure 11(b)**, **Figure 11(c)**).

(a)   (b)
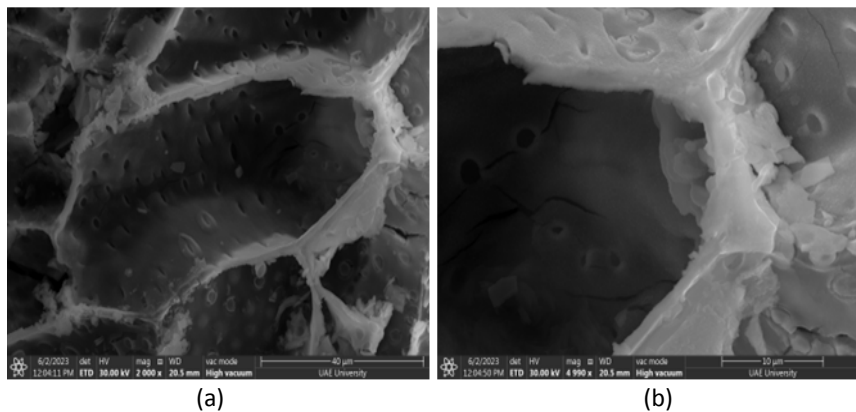
Figure 10. SEM micrograph of scale sample 4 at different magnification (a) X 2000, 40 μm and (b) X 5000, 10 μm.

(a)   (b)   (c)
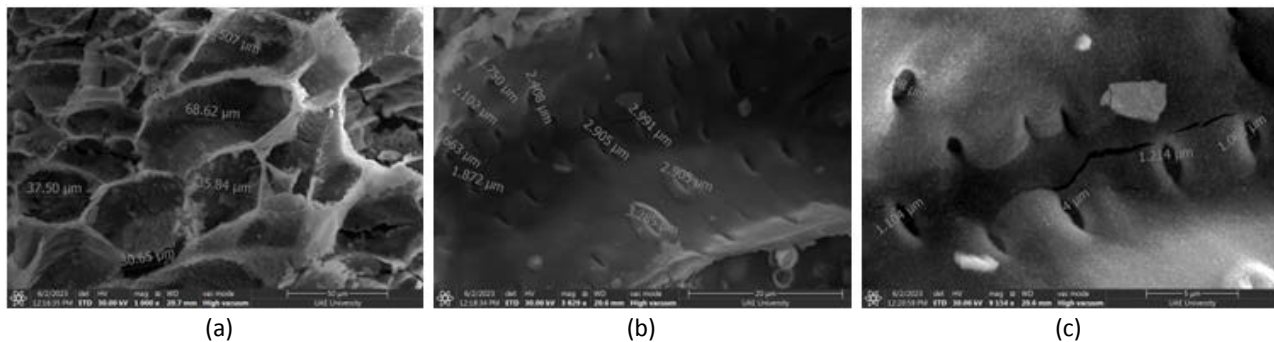
Figure 11. SEM image of pits and perforations of different sizes at different magnification. (a) X 1000, 50 μm, pit diameters range between 30 and 68 μm; (b) X 3829, 20 μm, pit diameters range between 1.66 and 3.28 μm; (c) X 9154, 5 μm, pit diameters range between 1.01 and 1.39 μm.

4. Discussion

The character of the produced water from the sour oil field causes extensive corrosion of the subsurface equipment including tubing. The corrosion is especially induced by the high chloride concentration. Of interest is the relative paucity of sulphur containing species measured in the collected produced water. Usually, H_2S distributes itself mainly over the gas fraction (Table 7), and a small amount (ca. 1v% of the total) remains in the hydrocarbon fraction. Although H_2S is soluble in water (3.98 g/L at 20˚C), its solubility decreases with increasing salinity of the water (about 2.5 g/L in seawater with TS of 35.000) [29]. Before the investigated produced water had been collected, flashing and stripping occurred, which would remove most of the H_2S present. However, the produced water was not specifically deaerated. Thus, the concentrations of sulphur species in the produced water do not reflect the concentrations of the sulphur containing molecules, including H_2S, that the tubing is exposed to. That these combined concentrations, especially when taking into account the H_2S concentration in the gas fraction (Table 7), are much higher, can be seen in the relatively high sulfur concentrations of the corrosion patina on the inner tubing.

The nature of the production fluid leads to extensive corrosion of the subsurface tubing with scalings blocking the production tubing. Scaling samples 1 - 4 collected from different blockages of the tubing have been found to be very heterogeneous (Table 4). In operating systems with a larger number of wells grouped around a central collecting unit the composition of the scalings will vary with which wells are operating at that moment and with what capacity. From XRD, it can be noted that the iron salts that make up part of the scaling are magnetite, hematite, greigite, siderite and goethite. Similar oxidation products from corrosion had been reported from the tubing from another Kuwaiti oilfield [8].

SEM images of debris stemming from the tubing that is part of the scaling show geometrically aligned rows of pits, which have partially progressed to the state of perforations. The pits and the perforations are not necessarily concentric, but have oblong shapes with the main axes aligned, most likely influenced by residual stress in the material.

Typically, tubing replacement happens every six months at a cost of $12.9 per tubing meter. This replacement contributes to the poor financial return of mature sour oilfields. In regard to mature oilfields, it must be kept in mind that a strategy needs to be in place to handle large amounts of produced water, and

Table 7. Typical composition of the gas fraction flowing through the tubing in the current case study, given in mole fraction %.

Methane (CH₄)	Carbon dioxide (CO₂)	Hydrogen sulfide (H₂S)	Nitrogen (N₂)	Ethane (C₂H₆)	Propane (C₃H₈)	Butane (C₄H₁₀)	Water (H₂O)
65%	12%	4%	0.5%	10%	5%	2.5%	1.0%

that in case of re-injection into the production well or in case of a general sub-surface disposal, an adequate treatment of such large amounts of water exists. Currently, both options, disposal, and injection, exist, although presently the produced water is pumped into a disposal well.

5. Conclusions

This contribution examined the impact of produced water from a sour oilfield in South Kuwait on the production tubing in the subsurface. It was noted that the heavily saline produced water leads to significant corrosion of the steel tubing discharging debris into the tubing. The debris can lodge in the tubing and was handled in this contribution as part of the scaling. The debris exhibited geometrically aligned corrosion pits, some of which had progressed to perforations. The used tubing itself showed a patina made up of iron oxides (such as hematite), iron carbonate (siderite) as well as iron sulfides (such as greigite). X-ray photoelectron spectra (XPS) of scaling samples, for the most part debris, showed that iron [Fe(0)] was still very much in evidence on the surface, along with Fe(II) and (Fe(III) species. Calcium salt deposits on the inner tubing at end of life made up of 2.6 w% the scaling directly adhering to the tubing. Silica deposits were also in evidence. The debris showed 0.75 - 9.3 w% Ca and 3.4 - 8.5 w% Si content.

In this type of operation, the produced water is either reinjected into the production well or is disposed in a disposal well. Especially in case of reinjection the produced water needs to be treated. The authors have not yet examined the above-ground tubing and the tubing used for reinjection or disposal. Nevertheless, it is recommended that produced water is treated at an early stage to minimize damage to above-ground and reinjection tubing. Lastly, produced water may represent a non-conventional water resource in addition to a source of industrial grade salt, if treated adequately.

Acknowledgements

Conflicts of Interest

The authors declare no conflicts of interest regarding the publication of this paper.

References

[1] Beyer, J., Goksøyr, A., Hjermann, D.Ø. and Klungsøyr, J. (2020) Environmental Ef-

fects of Offshore Produced Water Discharges: A Review Focused on the Norwegian Continental Shelf. *Marine Environmental Research*, **162**, Article ID: 105155.
https://doi.org/10.1016/j.marenvres.2020.105155

[2] Sutton-Sharp, E., Ravereau, J., Guennec, M., Brehant, A. and Bonnard, R. (2018) Benefits of Polymeric Membranes in Oil and Gas Produced Water Treatment. *Water Practice and Technology,* **13**, 303-311. https://doi.org/10.2166/wpt.2018.019

[3] Fakhru'l-Razi, A., Pendashteh, A., Abdullah, L.C., Biak, D.R.A., Madaeni, S.S. and Abidin, Z.Z. (2009) Review of Technologies for Oil and Gas Produced Water Treatment. *Journal of Hazardous Materials*, **170**, 530-551.
https://doi.org/10.1016/j.jhazmat.2009.05. 044

[4] Salem, F. and Thiemann, T. (2022) Produced Water from Oil and Gas Exploration—Problems, Solutions and Opportunities. *Journal of Water Resource and Protection*, **14**, 142-185. https://doi.org/10.4236/jwarp.2022.142009

[5] Ezennubia, V. ans Vilcáez, J. (2023) Removal of Oil Hydrocarbons from Petroleum Produced Water by Indigenous Oil Degrading Microbial Communities. *Journal of Water Process Engineering*, **51**, Article ID: 103400.
https://doi.org/10.1016/j.jwpe.2022.103400

[6] Abbas, A.J., Gzar, H.A. and Rahi, M.N. (2021) Oilfield-Produced Water Characteristics and Treatment Technologies: A Mini Review. *IOP Conference Series: Materials Science and Engineering*, **1058**, Article ID: 012063.
https://doi.org/10.1088/1757-899x/1058/1/012063

[7] Reike, D., Vermeulen, W.J. and Witjes, S. (2018) The Circular Economy: New or Refurbished as CE 3.0?—Exploring Controversies in the Conceptualization of the Circular Economy through a Focus on History and Resource Value Retention Options. *Resources, Conservation and Recycling*, **135**, 246264.
https://doi.org/10.1016/j.resconrec.2017.08.027

[8] Kamshad, T., Al-Ghamdi, A.R., Siritri, R.S. and Kellow, D. (2016) Risk Assessment for Implementation of Chemical Treatment Programs on Production Wells within the Wafra Oilfield Partition Zone (Kingdom of Saudi Arabia and Kuwait). Paper 7115, NACE International Source, CORROSION 2016, Vancouver, 6-10 March 2016.
https://onepetro.org/NACECORR/proceedings/CORR16/All-CORR16/NACE-2016-7115/123448

[9] Al-Hashem, A., Carew, J.A. and Al-Sayegh, A. (2000) The Effects of Water-Cut on the Corrosion Behavior L80 Carbon Steel under Downhole Conditions. Paper 00061, NACE International Source, CORROSION 2000, Orlando, 10-14 March 2000.
https://onepetro.org/NACECORR/proceedings/CORR00/All-CORR00/NACE-00061/111962.

[10] Scott, P.J.B., Al-Hashem, A. and Carew, J.A. (2007) Experiments on MIC of Steel and FRP Downhole Tubulars in West Kuwait Brines. Paper 07113, NACE International Source, CORROSION 2007, Nashville, 11-15 March 2007.
https://onepetro.org/NACECORR/proceedings/CORR07/All-CORR07/NACE-07113/126604

[11] Sun, W., Pugh, D.V., Ling, S., Reddy, R.V, Pacheco, J.L., Nisbet, R.S., Nor, N.M., Kersey, M.S. and Morshidi, L. (2011) Understanding and Quantifying Corrosion of L80 Carbon Steel in Sour Environments. Paper 11063, NACE International Source, CORROSION 2011, Houston, 11-15 March 2011.
https://onepetro.org/NACECORR/proceedings/CORR11/All-CORR11/NACE-11063/120595

[12] Smith, S. (2015) Current Understanding of Corrosion Mechanisms Due to H₂S in Oil and Gas Production Environments. Paper 5845, NACE International Source, CORROSION 2015, Dallas TX, 15-19 March 2015.
https://onepetro.org/NACECORR/proceedings/CORR15/All-CORR15/NACE-2015-5485/123229

[13] Li, Z.Y., Liao, W., Wu, W., Du, C. and Li, X. (2017) Failure Analysis of Leakage Caused by Perforation in an L415 Steel Gas Pipeline. *Case Studies in Engineering Failure Analysis*, **9**, 63-70. https://doi.org/10.1016/j.csefa.2017.07.003

[14] Li, X.G., Zhang, D.W., Liu, Z.Y., Du, C. and Dong, C. (2015) Materials Science: Share Corrosion Data. *Nature*, **527**, 441-442. https://doi.org/10.1038/527441a

[15] Stanley, R.K. (1998) An Analysis of Failure in Coiled Tubing. *IADC/SPE Drilling Conference*, Dallas, 3-6 March 1998, 515. https://doi.org/10.2118/39352-MS

[16] Crabtree, A.R. (2008) CT-Failure Monitoring: A Decade of Experience. *SPE/ICOTA Coiled Tubing and Well Intervention Conference and Exhibition*, The Woodlands, April 2008, SPE 113676, 1-7.

[17] Hoang, T.A., Ang, H.M. and Rohl, A.L. (2007) Effects of Temperature on the Scaling of Calcium Sulphate in Pipes. *Powder Technology*, **179**, 31-37.
https://doi.org/10.1016/j.powtec.2006.11.013

[18] Dyer, S.J. and Graham, G.M. (2002) The Effect of Temperature and Pressure on Oilfield Scale Formation. *Journal of Petroleum Science and Engineering*, **35**, 95-107.
https://doi.org/10.1016/S0920-4105(02)00217-6

[19] Pei, G., Wang, C. and Liu, L. (2014) Experimental Study on the Cause of Inorganic Scale Formation in the Water Injection Pipeline of Tarim Oilfield. Journal of Chemistry, 2014, Article ID: 619834. https://doi.org/10.1155/2014/619834

[20] Kardiman, Muryanto, S. and Bayuseno, A.P. (2015) Scaling of Calcium Carbonate (CaCO₃) in Pipes: Effect of Flow Rates and Tartaric Acid as Additives on Induction Time and Phase Transition. *Proceedings of the International Conference on Science and Science Education* (*IConSSE FSM SWCU)*, Salatiga, 1 August 2015, 71-77.

[21] Zhao, J., Liu, Y., Yang, X., He, X., Wang, L., Xiong, D. and Gu, Y. (2022) Corrosion Behavior of Pipeline Steel in Oilfield Produced Water under Dynamic Corrosion System. *Journal of Wuhan University of Technology—Material Science Edition*, **37**, 677-691. https://doi.org/10.1007/s11595-022-2582-3

[22] Chudyk, I., Poberezhny, L., Hrysanchuk, A. and Poberezhna, L. (2019) Corrosion of Drill Pipes in High Mineralized Produced Waters. *Procedia Structural Integrity*, **16**, 260-264. https://doi.org/10.1016/j.prostr.2019.07.050

[23] Liu, Y., Zhang, Y. and Yan, J. (2014) Influence of Produced Water with High Salinity and Corrosion Inhibitors on the Corrosion of Water Injection Pipe in Tuha Oil Field. *Engineering Failure Analysis*, **45**, 225-233.
https://doi.org/10.1016/j.engfailanal.2014.06.010

[24] AlAnezi, K., Al-Samhan, M., Belkharchouche, M., Abuhaimed, W., Alali, S., Alenizi, K. and Alfuraij, A. (2018) Comparative Analysis of Produced Water Collected from Different Oil Gathering Centers in Kuwait. *Journal of Environmental Protection*, **9**, 736-750. https://doi.org/10.4236/jep.2018.96046

[25] Li, W., Jing, J., Sun, J., Wang, S., Zhang, F. and Wang, H. (2023) Investigation of the Corrosion Characteristics and Corrosion Inhibitor Action on J55 Steel in Produced Water. *Sustainability*, **15**, Article 3355. https://doi.org/10.3390/su15043355

[26] Fan, J., Louie, S.M. and Rodrigues, D.F. (2018) The Influence of Salinity, pH, Temperature and Particles on Produced Water Oil Quantification Precision and Accuracy with Confocal Laser Fluorescence Microscopy. *Energy Fuels*, **32**, 6978-6989.

https://doi.org/10.1021/acs.energyfuels.8b01353

[27] Gaweł, B., Lesaint, C., Bandyopadhyay, S. and Øye, G. (2015) Role of Physicochemical and Interfacial Properties on the Binary Coalescence of Crude Oil Drops in Synthetic Produced Water. *Energy Fuels*, **29**, 512-519.
https://doi.org/10.1021/ef501847q

[28] Emam, E.A., Moawad, T.M. and Aboul-Gheit, N. (2014) Evaluating the Characteristics of Offshore Oilfield Produced Water. *Petroleum & Coal*, **56**, 363-372.

[29] Siang, H.Y., Tahir, N.M., Malek, A. and Isa, M.A.M. (2017) Breakdown of Hydrogen Sulfide in Seawater under Different Ratios of Dissolved Oxygen/Hydrogen Sulfide. *Malaysian Journal of Analytical Sciences*, **21**, 1016-1027.
https://doi.org/10.17576/mjas-2017-2105-03